

1        **Chemically-oscillating reactions in the formation of botryoidal malachite**

2

3

Dominic Papineau

4

London Centre for Nanotechnology, Department of Earth Sciences, and Center for Planetary Science, University

5

College London, London, U.K.

6

7        **Abstract**

8

The origin of banding patterns in malachite [Cu<sub>2</sub>CO<sub>3</sub>(OH)<sub>2</sub>] is an enduring problem in  
9 geology. While the bright green vivid colors of this mineral have been attributed to the presence  
10 of Cu, no specific process has been proposed that can explain the perfect circularly concentric  
11 banding and geometrical shapes in botryoidal malachite. These patterns of concentric equidistant  
12 laminations are comparable to those arising from chemically-oscillating experiments using the  
13 classical reactants of the Belousov-Zhabotinsky (B-Z) reaction. Through optical microscopy and  
14 micro-Raman imaging, this contribution documents that the geometric centers of the self-similar  
15 geometric patterns are often composed of organic matter. Carbon isotopes and trace elements  
16 further suggest that non-biological decarboxylation reactions of biological organic matter took  
17 place during diagenesis. Hence, the morphological and chemical characteristics of chemically-  
18 oscillating reactions offer a plausible explanation for the formation of botryoidal malachite and  
19 abiotic environmental decarboxylation reactions.

20

21

22        Keywords: Malachite, botryoids, Belousov-Zhabotinsky reaction, organic matter, Raman,  
23        decarboxylation

24

25

## **Introduction**

26

27 Mineral banding is a common feature of mineral overgrowth during precipitation from  
28 aqueous solutions and microbial growth. Episodic growth leads to single crystals with concentric  
29 euhedral layers representing the age and composition of each generation of fluids, such as  
30 metamorphic zircons. However, this process does not predict that crystal habits or banding  
31 should have circularly concentric and radial geometries, such as in botryoidal malachite. The  
32 geometric shape of malachite can be modelled as a ‘surface normal growth’ phenomenon, based  
33 on a non-linear equation that plots cusps between smooth spheroids (Jettestuen et al., 2006). It  
34 has also been suggested that such geometric patterns grow heterogeneously, as a function of  
35 time, and influenced by some external processes triggering nucleation (Jamtveit and Hammer,  
36 2012). While mathematical models can make progress, the enigma of the natural process leading  
37 to malachite banding and its occurrence as bunches of grapes is an enduring puzzle. This  
38 phenomenon is also relevant for biosignatures because stromatolite-like botryoidal growths  
39 commonly occur in malachite, yet their occurrence in nature is generally inconsistent with photic  
40 environments required for a photosynthetic microbial origin. In fact, botryoidal malachite  
41 generally occurs as crusts inside cavities in country rocks affected by supergene, briny, and Cu-  
42 rich fluids. Indeed, malachite is usually thought to be hydrothermal alteration or a secondary  
43 mineral developed from the weathering of other minerals. Yet, no theory fully explains the origin  
44 and shape of its distinct and notable banding.

45

46 At the start of the twentieth century, new diffusion experiments in silica gels showed the  
47 development of periodic layering due to diffusion, a pattern referred to as Liesegang banding

***Earth in five Reactions Special Collection***

Papineau

Revision 1

48 (Liesegang, 1910, 1915). The original idea put forward to explain the periodic colour layering  
49 was due to metal cation impurities diffusing in silica gel, which creates color gradients in objects  
50 like agate geodes (Liesegang, 1910). This phenomenon was subsequently proposed to explain  
51 banding in malachite (Hartman et al., 1934). Indeed, the appearance of Liesegang bands in silica  
52 gel is similar to some patterns exhibited by natural agates and chalcedony in geodes from  
53 volcanic terrains (Götze, 2011). However, most patterns in malachite and geodes are rounded as  
54 opposed to linear such as in Liesegang banding, hence this type of diffusion does not explain the  
55 geometry of botryoids. Therefore, current explanations for the origin of banding in malachite are  
56 incomplete.

57

58         The Belousov-Zhabotinsky reaction (B-Z reaction from hereon) is spontaneous under  
59 standard conditions and involves the oxidation of carboxylic acids (such as malonic acid –  
60  $C_3H_4O_4$ ) by a strong oxidizer and its corresponding halide salt (such as the oxidized halogen  
61 bromate and its halide salt bromide), as well as a strong acid (such as sulfuric acid; Belmonte,  
62 1997; Orbán et al., 2001). When using metal-bearing redox-sensitive dye, such as ferroin  
63 (phenanthroline ferrous sulfate –  $C_{12}H_8FeN_2O_4S$ ), this decarboxylation reaction becomes notable  
64 and unique as it produces characteristic self-similar patterns of circularly-concentric chemical  
65 waves (Zaikin and Zhabotinsky, 1970). Over minutes time scales, these chemical waves are  
66 displayed as blue-purple, circular, concentric and equidistant waves that propagate radially and  
67 periodically from randomly located spots in the orange-colored solution. Bubbles of  $CO_2$   
68 eventually form from the cleavage of carboxyl functional groups from malonic acid. Hence, the  
69 B-Z reaction is an out-of-equilibrium, spontaneous, cyclic, patterns-forming, and oxidation-  
70 reduction reaction. A new hypothesis can thus be posed for the origin of banding in malachite:

***Earth in five Reactions Special Collection***

Papineau

Revision 1

71 chemically-oscillating reactions participated in the formation of these enigmatic self-similar  
72 patterns. In this contribution, the botryoidal habit and geochemical composition of malachite are  
73 compared to the patterns and composition of chemically-oscillation reactions.

74

75

**Materials and methods**

76

*Chemically-oscillating reactions*

77

78

79

80

81

82

83

84

85

86

87

88

89

90

91

92

93

To study the detailed self-similar patterns of the B-Z reaction, more than sixty experiments performed in 10 cm diameter glass Petri dishes were imaged using the following reactants: 6 ml of (1M) NaBrO<sub>3</sub> mixed with (0.33M) H<sub>2</sub>SO<sub>4</sub>, 0.5ml of (1M) NaBr, 1ml of (1M) malonic acid, 1ml of (25mM) Ferroin (phenanthroline ferrous sulfate; Reagecon), and a drop of dilute triton X-100. The first three solutions are mixed until the yellow color disappears, which takes approximately 2 minutes of gentle stirring, and the ferroin redox indicator and dilute soap are then added. A bicolor orange-blue spontaneously forms upon contact with the solution and homogenization yields a first-order time-period oscillation of orange-blue colors for the entire Petri dish. If the solution is continuously stirred, the homogenized colored background will oscillate between orange-red and purple-blue, because stirring accelerates this longest time-period, and thus first-order, oscillation frequency. However, if the homogenous solution is left unstirred, a series of chemical waves diffuse through the solution and repeat over times scales of minutes until the Petri dish is filled with the blue color (typically after more than 20 minutes). Experiments were performed on countertops in ambient temperatures varying between about 20 and 25°C most often in a fume hood and on an LED-illuminated light bench. The reaction is spontaneous and out-of-equilibrium and the pattern development lasts between about 45 and 75 minutes, depending on the number of resets (i.e. when the solution is gently stirred until the next

***Earth in five Reactions Special Collection***

Papineau

Revision 1

94 homogeneous orange background is re-established). Data was collected using various CCD  
95 cameras in both photo and video modes and only representative images are shown.

96

97 *Comparative analyses of malachite botryoids by optical microscopy and micro-Raman*

98 For the comparison of patterns in botryoidal malachite with those in the B-Z reaction,  
99 specimens in private collections were photographed and one was selected for petrographic  
100 analysis in thin section. Optical microscopy was thus performed on three thin sections of the  
101 botryoidal malachite from the Katanga locality in the Central African Copper Belt in the  
102 Democratic Republic of Congo. A BX-51 Olympus petrographic microscope located at UCL was  
103 used to collect transmitted and transmitted plus reflected images with the following objectives:  
104 5x, 10x, 20x, 50x, and 100x. A condensing lens was used for all images. Oil immersion or ink  
105 markings were not used on the polished thin sections, which were cleaned by gently rubbing an  
106 acetone-wetted kimwipe.

107 A WITec  $\alpha$ 300 micro-Raman system at UCL was used to image organic matter in  
108 botryoidal malachite. Micro-Raman was performed using a 532 nm laser set at 8 mW, and  
109 according to previously described techniques (Papineau et al., 2011; 2016). An optic fiber of 50  
110 microns in diameter was used to collect the inelastically-scattered photons, which were dispersed  
111 through a 600 l/mm grating, thus resulting in a spectral resolution of 4  $\text{cm}^{-1}$ . The spatial  
112 resolution was set at one pixel per two microns, whereas the acquisition time on each pixel was  
113 0.4 seconds, for a total of 84,100 spectra collected (290 x 290 pixels). Hyperspectral images are  
114 created using color-coded using the strongest unique peak of all phases present: malachite in  
115 green (filter center = 1495 $\text{cm}^{-1}$ , width = 20 $\text{cm}^{-1}$ ), quartz in blue/purple (filter center = 466 $\text{cm}^{-1}$ ,  
116 width = 30 $\text{cm}^{-1}$ ), anatase in yellow (filter center = 143 $\text{cm}^{-1}$ , width = 25 $\text{cm}^{-1}$ ), organic matter in

***Earth in five Reactions Special Collection***

Papineau

Revision 1

117 red (filter center =  $1583\text{cm}^{-1}$ , width =  $120\text{cm}^{-1}$ ), and an unknown phase in dark red (filter center  
118 =  $596\text{cm}^{-1}$ , width =  $200\text{cm}^{-1}$ ).

119

120

*Bulk geochemical analyses of malachite*

121 Powder of malachite was prepared using a steel mortar and pestle, which was prepared  
122 with the following steps: cleaned using soap and plastic brush, DI water rinses, acetone rinse,  
123 muffled quartz chips ( $600^{\circ}\text{C}$  for 4 hours in air) crushed to very fine powder, rinsed again with DI  
124 water, and finally air-dried. Malachite powder was transferred to muffled clear borosilicate glass  
125 vials (also 4 hours at  $600^{\circ}\text{C}$ ). Plastic caps were soaked in 10% HCl for 24 hours, followed by DI  
126 water rinses and air drying.

127

128 For bulk analysis of trace elements,  $\sim 0.1\text{g}$  of powder was initially heated in mixture of  
129 1.0 ml hydrochloric acid (37% w/v; analytical grade), 1.0 ml nitric acid (69% w/v; analytical  
130 grade), and 0.5 ml hydrofluoric acid (40% w/v; analytical grade) at  $110^{\circ}\text{C}$  for 16 hours. The  
131 solution was evaporated to incipient dryness before addition of 2.0 ml  $\text{HNO}_3$  and 0.5 ml  $\text{HClO}_4$   
132 (70% w/v; analytical grade), which was again evaporated to incipient dryness. A further 1 ml  
133 aliquot of  $\text{HNO}_3$  was evaporated and the residue dissolved in 100 ml of 1.0%  $\text{HNO}_3$  prior to  
134 analyses by ICP-OES and ICP-MS at University College London. Data is reported in Table 2,  
135 which shows elemental abundances determined by ICP-OES as concentrations in ppm and % and  
136 by ICP-MS as concentrations in ppb. Analyses of certified reference material NBS120b (Florida  
137 Phosphate Rock) yielded recoveries above 95%. Bulk analyses of carbon isotopes were also  
138 performed at UCL using previously used techniques (Papineau et al., 2013), that included a Gas

***Earth in five Reactions Special Collection***

Papineau

Revision 1

139 Bench for bulk malachite carbonate and an Elemental Analyzer for organic matter in HCl-  
140 dissolved malachite, both linked to a Thermo Delta V isotope ratio mass spectrometer.

141

142

**Results**

143

*Dimension and time-scale of patterns in chemically-oscillation reactions*

144

145

146

147

148

149

150

151

152

153

154

155

156

157

158

159

160

161

Self-similar patterns are formed by the diffusion of reaction products, and these chemical waves are erased when they intersect each other through a process of destructive interference. It is noted however that typical patterns of destructive interference from interacting circular waves yield discontinuous circular wave lines (e.g. a double-slit diffraction pattern by a plane wave), whereas chemically-oscillating reactions are unique in showing that waves interfere destructively by erasing the wave trace at their intersection. Self-similar patterns in the B-Z reaction include the morphologies listed in (Table 1) and generally described as accumulations of myriad perfect, circularly-concentric, and equidistant laminations (Fig. 1a (pl. 2&3); Fig. 1e (pl. 1)). In most experiments, oxidation spots have circularly-concentric laminations that are only slightly imperfect with diameters spanning sub-millimeter to decimeter sizes (Fig. 1a (pl. 2); Fig. 1i (pl. 3)). Concentric spots can also have slightly imperfect equidistant or non-equidistant laminations (Fig. 1e (pl.2-3)), or they can be asymmetric irregular ellipses of chemical waves or with variable spacing distance (Fig. 1a (pl. 4)). Some chemical waves initiate from the edge of the Petri dish, which may be triggered by surface tension or invisible impurities on the borosilicate glass. This can lead to the formation of a cavity-shaped structure progressively closing outside-in (Fig. 1a (pl. 1)). Other notable and distinct morphological traits include parallel-layered to wavy patterns with intersecting oxidation spots (Fig. 1g (pl. 1&2)), columnar-turbinate (stromatolite-like) laminated patterns (Fig. 1g (pl. 4)), and strong color gradients in laminations can be associated

***Earth in five Reactions Special Collection***

Papineau

Revision 1

162 with a diffused spotted texture filling the orange background (Fig. 1g (pl. 3); Fig. 1i (pl. 1-2)).  
163 Rarely, oxidation spots display a globular texture where the spheroids have a pronounced color  
164 gradient rather than concentric circular laminations (Fig. 1c (pl. 1-4)).

165 Bubbles of CO<sub>2</sub> produced during these chemically-oscillating decarboxylation reactions  
166 generally remain attached to the Petri dish and grow over time to sizes more than 1mm in  
167 diameter (Fig. 1e (pl. 2)). The patterns change from one experiment to another, but they have the  
168 same self-similar characteristics as the concentric patterns described above: circularly-concentric  
169 waves that periodically expand radially and display a color gradient. Notably in several  
170 experiments, the spotted background oscillates with a different, faster, third-order time-period,  
171 distinct from the second-order chemical oscillations located in discrete oxidation spots (e.g. Fig.  
172 1i (pl.1-2)). The oscillations in the blue and orange colors are thus represented by at least three  
173 orders of time periods: a first-order of pattern formation as completely filled with blue and  
174 reverting to its original orange background with a time-period on the order of about 20-30  
175 minutes, a second-order of pattern formation with sub-millimetric to decimetric oxidation spots  
176 with chemical waves that have periods on the order of about 30 to 90 seconds, and lastly a third-  
177 order of pattern formation (present in less than about 10% of experiments) with sub-millimetric  
178 to millimetric spots or convex lined patterns that have periods on the order of 10 to 20 seconds.

179

180 *Optical analysis of patterns in malachite botryoids*

181 Botryoidal malachite exhibits randomly-located concentric spheroids with perfectly to  
182 imperfectly equidistant laminations with gradients of shades of green (Fig. 1b (pl. 1&2)). At the  
183 decimeter to millimeter scales, various polished cross-sections of malachite have these kinds of  
184 laminations that form spots with perfect to imperfect, merging lines of concentric laminations



***Earth in five Reactions Special Collection***

Papineau

Revision 1

185 that form concretionary cavity-structures or imperfect concentric-layered spheroids (Fig. 1b  
186 (pl. 1-3)). This particularly distinguishing feature in self-similar patterns of malachite can also be  
187 described as cavity-shaped structures formed from the merging of rounded concentric waves that  
188 have had their trace erased through a process of destructive interference (Fig. 1f (pl. 2)). This  
189 important morphological characteristic of malachite has never been explained, yet it is identical  
190 to some features observed in chemically-oscillating reactions (Fig. 1e (pl. 4)). The laminations of  
191 malachite vary from perfect, circularly-concentric and equidistant laminations (Fig. 1f (pl. 1-3)  
192 and Fig. 1b (pl. 3)) to slightly imperfect, sub-rounded, non-equidistant laminations (Fig. 1b (pl.  
193 1); Fig. 1h (pl. 3)). A particularly intriguing morphological features in malachite is the  
194 occurrence of convex-upward columnar-turbinate laminated pattern analogous to some columnar  
195 stromatolites (Fig. 1h (pl. 1)). Strong color gradients also occur in laminations that can be  
196 associated with diffused spotted texture (Fig. 1j (pl. 1)). Table 1 summarizes the similar  
197 morphological traits observed in cross-sections of malachite and in chemically-oscillating  
198 reactions.

199

200 When viewed in three dimensions, the malachite spheroids are generally of similar size  
201 and similar to grapes with spheroidally-concentric shells (Fig. 1d). Close examination under the  
202 optical microscope reveals geometrically perfect laminations that are sometimes truncated and  
203 discontinued. These appear as symmetric patterns with morphologies including perfectly  
204 concentric spots, open-book-like, and microscopic spherical rosettes (Fig. 1b, 1f, 1j). Self-similar  
205 macroscopic structures that emerge from these layers form columnar turbinate stromatolite-like  
206 structures, pillars with rounded-convex and hollow-concave ends, or outward-growing turbinate  
207 fans (Fig. 1h). When malachite forms linear layers, there are still perfect concentric-layered

208 spheroids that span sizes between about 1 cm to ca. 0.1 mm (Fig. 1j). These spheroids form  
209 layers that grow inside rock cavities or on bedding planes. These observations demonstrate the  
210 existence of 3-D self-similar patterns in malachite that include circularly-concentric laminations,  
211 color gradients, randomly localized spots, and structures similar to rosettes, grapes, stromatolites,  
212 or cavities. Hence, the same kinds of self-similar patterns are observed in both in botryoidal  
213 malachite and in chemically-oscillating reactions.

214

215

*Organic matter in malachite botryoids*

216 Cross-sections of Katanga malachite reveal an abundance of fine perfectly equidistant  
217 laminations, sometimes with organic-rich layers (Fig. 2a) or forming turbinate columnar  
218 structures with color gradients varying from green to black-green (Fig. 2b-2c). Dendritic to  
219 arborescent opaque masses of organic matter are commonly located in the geometric center of  
220 malachite botryoids (Fig. 2d). Reflected light images reveal the occurrence of vugs inside the  
221 arborescent organic matter (Fig. 2e), whereas transmitted light images reveal laminations and  
222 bulbous protuberances (Fig. 2d, 2f). The bulbous protuberances also occur in the geometric  
223 center of smaller patterns of circularly-concentric laminations of carbonate (white arrows in Fig.  
224 2f). The arborescent organic masses span sizes between about 500 to 1000  $\mu\text{m}$ .

225 Micro-Raman imaging confirms the composition of organic matter with a poorly-  
226 resolved D1 peak at around  $1345\text{ cm}^{-1}$  and a better-resolved G-peak at  $1583\text{ cm}^{-1}$  (Fig. 2h)  
227 characteristic of low-grade metamorphic sedimentary organic matter such as kerogen. Raman  
228 spectra of organic matter show two types of crystallinity, with either a poorly-resolved or an  
229 unresolved D1 peak. This organic matter is also closely associated with layers more than 100  $\mu\text{m}$   
230 in thickness of another, unidentified phase with a broad peak at  $596\text{ cm}^{-1}$ , possibly umber-like

***Earth in five Reactions Special Collection***

Papineau

Revision 1

231 (Fig. 2g). The spectra of organic matter are relatively noisy and there are no 2D peaks in the  
232 2600-3000  $\text{cm}^{-1}$  region, as would be expected from kerogen (Schopf and Kudryavtsev, 2009).  
233 The Raman spectrum of malachite shows medium intensity peaks for carbonate at 1062 and 1098  
234  $\text{cm}^{-1}$ , along with peaks at 218, 271, 348, 434, 537, 720, 752, and 1495  $\text{cm}^{-1}$ , and the OH peak at  
235 3382  $\text{cm}^{-1}$  (Fig. 2h). This is similar to the peak distribution of Namibian malachite  
236 (ruff.info/malachite), which has peaks at 219, 268, 345, 431, 533, 717, 750, 1060 and 1095  $\text{cm}^{-1}$ .  
237 Micro-Raman imaging also reveals the presence of anatase crystals a few microns in size  
238 inside the organic matter adjacent to the coarse-grained quartz at the root of the arborescent  
239 structure (Fig. 2g).

240

241 *Bulk composition of Katanga malachite*

242 Major elements in the Katanga malachite include Cu at 55.3% and P at 4.3% (Table 2).  
243 Trace elements are dominated by Al, Mn and Zn, which occur at concentrations of 401, 585, and  
244 890 ppm, respectively (Table 2). Divalent cations such as Ba, Ca, Co, Cr, Fe, Mg, and Ni occur  
245 in concentrations of 40, 39, 200, 0.6, 85, 163, and 18 ppm, respectively. For halogens, I occurs in  
246 a concentration of 1.1 ppm, whereas Br is at 10.9 ppm. Rare Earth Elements (REE) occur in low  
247 concentration (total REE = 11.8 ppm) and form a trend of higher abundance for heavy REE and  
248 lower abundance for light REE. Lastly, the bulk malachite powder was found to contain organic  
249 matter with a  $\delta^{13}\text{C}_{\text{org}}$  value of -28.6‰, in comparison with the carbonate which has a  $\delta^{13}\text{C}_{\text{carb}}$   
250 value of -10.6‰ and  $\delta^{18}\text{O}_{\text{carb-PDB}}$  value of -5.1‰ (Table 2).

251

252 **Discussion**

253 **From aqueous solution to mineralization**

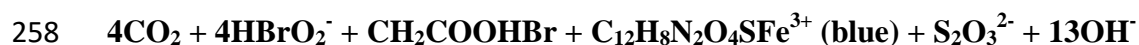
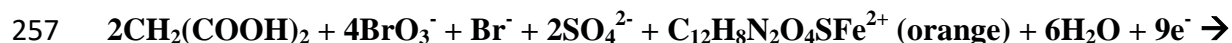
***Earth in five Reactions Special Collection***

Papineau

Revision 1

254 The following chemically-balanced equation represents the decarboxylation of malonic  
255 acid by reactants used in this work and some expected products:

256



259

260 This oxido-reduction reaction is catalyzed by redox-sensitive ferroin mediated by interaction  
261 between malonic acid and halogen compounds because halogens especially react with carboxyl  
262 groups in organic acids, leading to the formation of halogenated organic molecules. As carbon  
263 dioxide can precipitate carbonates at equilibrium under slightly alkaline pH, the above equation  
264 suggests that both  $\text{CO}_2$  and alkalinity are created by the oxidation of malonic acid. Various  
265 intermediates are expected or predicted, such as bromomalonic acid ( $\text{CH}_2\text{COOHBr}$ ), bromous  
266 acid ( $\text{HBrO}_2$ ) and thiosulfate ( $\text{S}_2\text{O}_3^{2-}$ ). Electrochemical analyses have demonstrated that a voltage  
267 potential exists between chemical waves and thus that an electron motive force is generated from  
268 chemically-oscillating reactions (Zhabotinsky, 1991). Measurements of  $\text{Br}^-$  concentration in the  
269 B-Z reaction also show that it varies in periodic oscillations and that the redox potential between  
270 the  $\text{Br}^-$  and  $\text{BrO}_3^-$  is 1.44 V (Körös and Orbán, 1978). This chemical potential acts to transfer  
271 electrons until either there are no more terminal electron acceptors (bromate and sulphate) or no  
272 more electron donor molecule (organic acids). The energy created by the reaction is responsible,  
273 in part, for the diffusion of reaction products away from oxidation spots, however the  
274 mechanisms of pattern initiation and development at the microscopic and nanoscopic scales  
275 remain to be documented. In nature, for as long as the solution pH is slightly alkaline and  
276 divalent cations are available in diagenetic pore water solutions,  $\text{CO}_2$  could precipitate carbonate

***Earth in five Reactions Special Collection***

Papineau

Revision 1

277 minerals as micrite. Diffusing chemical waves with variable oxidation states could conceivably  
278 be immobilized in lithifying malachite micrite and contribute to the formation and crystallization  
279 of circularly-concentric and radially-aligned malachite crystals (e.g. Fig. 2d). For instance, gels  
280 of N-isopropylacrylamide and polyacrylamide-silica composites have been used with success to  
281 immobilize chemical waves in B-Z reactions (Chou Chen et al., 2011). It is therefore suggested  
282 that hydrated micritic malachite could allow diffusion of chemical waves, and lithification could  
283 immobilize them, although this still awaits experimental demonstration.

284 Experiments have shown that chemically-oscillating reactions can take place under  
285 variable ranges of reactant concentrations: 0.15-2.0 M H<sub>2</sub>SO<sub>4</sub>, 0.075-0.4 M NaBrO<sub>3</sub>, and 0.05-  
286 0.8 M malonic acid (Körös and Orbán, 1978; Agladze et al., 1984; Belmonte et al., 1997). In  
287 fact, there are also various other organic acids that can be used for chemically-oscillating  
288 reactions including mono- and di-carboxylic acids and ketones (Belmonte et al., 1997; Orbán et  
289 al., 2001). Similarly, chemical oscillations have also been observed using various kinds of strong  
290 oxidizers such as iodate, bromate, and hydrogen peroxide (Briggs and Rauscher, 1972; Epstein et  
291 al., 1983). Several strong acids have also been used such as hypophosphite, arsenate, and sulfuric  
292 acid, and catalysts such as Mn<sup>2+</sup>, Ce<sup>3+</sup>, Fe<sup>2+</sup>, Ru<sup>2+</sup>, Cr<sup>2+</sup>, Co<sup>2+</sup>, Fe(phen)<sub>3</sub><sup>2+</sup> (ferroin), Ru(bpy)<sub>3</sub><sup>2+</sup>  
293 (ruthenium) have also been used to generate patterns in chemically-oscillating reactions  
294 (Belmonte et al., 1997; Orbán et al., 2001). In the Katanga malachite, most of these compounds  
295 occur (Table 2) and it is possible they could have contributed to chemical oscillations. The  
296 oxidation state of Cu in malachite is well-established to be +2 and Cu is a metal that can be  
297 halogenated by Br and I (Hemachandran and Chetal, 1986). Hence, since both Br and I occur in  
298 ppm levels in the Katanga malachite, a possible scenario could also involve Cu<sup>+1</sup> and Cu<sup>0</sup> during  
299 diagenetic and supergene conditions, which could potentially contribute to the abiotic

***Earth in five Reactions Special Collection***

Papineau

Revision 1

300 decarboxylation of biomass. Unfortunately, in the absence of experimental evidence, the exact  
301 physical-chemical conditions during which botryoidal malachite forms are not known. Hence,  
302 the discussion shall now explore the similarities between the geometry of self-similar patterns in  
303 the chemically-oscillating reactions and in botryoidal malachite, and then focus on the organic  
304 matter in malachite.

305

306 **On the origin of concentric fractal pattern morphologies**

307 Self-similar patterns in chemically-oscillating experiments include cavity-shaped  
308 structures, perfectly to imperfectly circularly-concentric and equidistant laminations, columnar  
309 turbinate structures, color gradients in chemical waves, and various spotted, globular, zebra-  
310 striped, and fingerprint-like patterns (Table 1). The B-Z reaction is also known to produce spiral-  
311 like patterns inside concentric equidistant laminations (Agladze et al., 1984; Belmonte et al.,  
312 1997). Not all these patterns are documented in botryoidal malachite. For instance, no distinct  
313 spirals, zebra-striped or fingerprint-like patterns have been observed in malachite, in the  
314 knowledge of the author. However, the proliferation of spots in the B-Z reaction (Fig. 1i (pl.  
315 1&2)) is reminiscent of the myriad small rounded concentric spots and rosettes found in  
316 botryoidal malachite (Fig. 1j (pl. 1&2)). In B-Z experiments, the zebra-pattern exhibited in  
317 association with turbinate columns (Fig. 1g, pl. 4) and the globular spots (Fig. 1c (pl. 1-3)) are  
318 morphologies akin to columnar turbinate pattern in stromatolitic malachite (Fig. 1h (pl. 1), 2b,  
319 2c) and to grape-shaped malachite botryoids (Fig. 1d), respectively. Truncated and discontinuous  
320 laminations in the B-Z reaction (Fig. 1e (pl. 4)) are akin to those in malachite (Fig. 1f (pl. 1-2))  
321 and can be explained by a process of destructive interference of radially-expanding chemical  
322 waves, which suggests that similar processes underlie the formation of such structures.

***Earth in five Reactions Special Collection***

Papineau

Revision 1

323 Circularly-concentric, equidistant laminations with color gradients and sizes between sub-  
324 millimeter to decimeter in B-Z experiments (Fig. 1a (pl. 2), 1e (pl. 1); 1i (pl. 3)) are identical to  
325 perfectly concentric malachite spheroids from decimetric botryoids to microscopic rosettes (Fig.  
326 1b (pl. 1), 1d (pl. 2), 1f (pl. 3), 1j (pl. 2-3)). In summary, there are several forms of self-similar  
327 patterns in chemically-oscillating reactions that share morphologies identical to those in  
328 botryoidal malachite.

329 Mathematically, the changing patterns in chemically-oscillating reactions can be  
330 described using well-known equations such as Euler's formula (including Euler's identity),  
331 Fourier transform, the Navier-Stokes equation, and the wave equation. The Navier-Stokes  
332 equations illustrate the motion of viscous fluid substances, and they have been used to model  
333 fluid flow and diffusion processes like the B-Z reaction (Kitahata et al., 2002). Spherical waves  
334 oscillating from point sources can be represented by an n-dimensional wave equation: for the B-  
335 Z reaction, that partial differential equation would describe the time-dependent scalar function of  
336 particle motion in 3-D space as an oscillating function from randomly located point sources. The  
337 periodicity or frequency of the chemical waves is related to time through Fourier transform.  
338 Lastly, Euler's identity ( $e^{i\pi} + 1 = 0$ ) is an ideal solution to Euler's formula, which equates a unit  
339 complex number ( $e^{i\phi}$ ) to the trace of a unit circle in a complex plane. It can then be suggested  
340 that these equations might have a solution related to the types of geometries and periodic  
341 oscillations observed in both the B-Z reaction and in malachite botryoids. One also needs to  
342 consider the fact that many forms in nature can be described by fractals and that mathematical  
343 models of B-Z geometric patterns are complex. Minerals are a fundamental type of fractal where  
344 the unit cell repeats over several dimension scales in a geometric pattern defined by 4 polygonal  
345 shapes (with 2, 3, 4, or 6 sides), 14 Bravais lattices, 32 point groups, and 230 space groups.

***Earth in five Reactions Special Collection***

Papineau

Revision 1

346 Mathematical fractals might form botryoidal chalcedony through Mandelbrot-like pattern growth  
347 (Brasier et al., 2005), manganiferous dendrites have been modelled as two-dimensional  
348 Laplacian-type growth fractals (Garcia-Ruiz, 1994; Seilacher, 2001), and deep-sea stromatolitic  
349 manganese nodules can be modelled as fractal aggregates of polyhedra (Akai et al., 2013).  
350 Future work should compare the mathematical modelling of patterns in chemically-oscillating  
351 reactions with those in malachite.

352         While mathematics constitutes one approach to contribute to the problem of the origin of  
353 botryoidal malachite, this mineral has also not yet been experimentally synthesized in the  
354 laboratory. Low-temperature supergene conditions have been inferred from the mode of  
355 occurrence of malachite in rocks. The exact formation process remains unknown, but it could  
356 have involved some of the metals detected in the bulk composition such as Cu, P, Zn, Mn, Co,  
357 and V, because these can all have variable oxidation states and they are all relatively abundant in  
358 the Katanga malachite. In addition, the presence of bromine and iodine in malachite is consistent  
359 with these compounds having been involved in its formation. This new information could be  
360 useful for future malachite synthesis experiments under supergene-like low-temperature  
361 conditions.

362

363         **Organic matter from biomass as a reactant in geological chemically-oscillating reactions**

364         New observations by optical microscopy and micro-Raman imaging of malachite from  
365 Katanga show the occasional presence of organic matter located in the geometric centers of  
366 concentric features (Fig. 2d-2f). This organic matter is highly heterogeneous in the bulk rock and  
367 has a  $\delta^{13}\text{C}_{\text{org}}$  value of -28.6‰ consistent with biological fractionation, whereas bulk malachite  
368 has a  $\delta^{13}\text{C}_{\text{carb}}$  value of -10.6‰ consistent with the oxidation of organic matter. In fact, similar



***Earth in five Reactions Special Collection***

Papineau

Revision 1

369 <sup>13</sup>C-depleted compositions for organic matter and carbonate are common in sedimentary  
370 concretions and in banded iron formations where they are thought to represent oxidized biomass  
371 (Plet et al., 2016; Dodd et al., 2019). Hence, the C-isotope compositions of organic matter and  
372 carbonate in the Katanga malachite are independent signatures for the decarboxylation and  
373 oxidation of biomass. This is also akin to some agate geodes that have comparable, circularly-  
374 concentric, and self-similar patterns as well as bitumen (Gaweda and Rzymelka, 1992). Agate  
375 geodes also have <sup>13</sup>C-depleted carbonate (Götze et al., 2015; 2011), and/or have various volatile  
376 compounds as fluid inclusions including NO, SO, CO<sub>3</sub><sup>2-</sup>, CH, and HF (Richter-Feig et al. 2018).  
377 The latter signatures in agate geodes can thus also be used to suggest that inorganic acids  
378 contributed to produce <sup>13</sup>C-depleted carbonate during the oxidation of <sup>13</sup>C-depleted organic  
379 acids. Organic matter of biological origin and inside concretions is usually rich in -COOH  
380 groups, which are known to be removed through decarboxylation during diagenesis and  
381 metamorphism (Bernard et al., 2007). This source of CO<sub>2</sub> is thus <sup>13</sup>C-depleted and can mix with  
382 variable amounts of seawater carbonic acid. The petrographic relationship between the organic  
383 matter and botryoids is consistent with the interpretation that the organic matter was  
384 decarboxylated in oxidizing and Cu-rich fluids. Lastly, the co-occurrence of anatase in the  
385 dendritic organic matter is also consistent with other reports of the presence of TiO<sub>2</sub> with fossil  
386 biomass, including in Paleoproterozoic botryoids and stromatolites (Djokic et al., 2017), and  
387 Paleoproterozoic microfossiliferous apatite granules (Papineau et al., 2017).

388 The arborescent masses of organic matter in malachite are similar to structures referred to  
389 as *Frutexites*. *Frutexites* microfossils often appear to be associated with evidence for the  
390 putrefaction of biomass, such as their bulbous arborescent growth directly onto animal fossils.  
391 For instance, *Frutexites* are seen in Cretaceous brachiopods, bivalves, belemnites, and ostracods

***Earth in five Reactions Special Collection***

Papineau

Revision 1

392 from Norfolk in the United Kingdom (Andrews et al., 2015), Jurassic foraminifera from the  
393 Betic-Rifian Cordillera in Spain (Reolid, 2011), and Devonian rugose corals from the eastern  
394 Anti-Atlas in southern Morocco (Jakubowicz et al., 2014). These microbial structures also occur  
395 in Late Paleoproterozoic stromatolites from Western Ontario in Canada (Walter and Awramik,  
396 1979), and in modern concretionary structures of zeolite from the Mariana Trench seafloor (Peng  
397 et al., in review). *Frutexit*s are commonly dominated by organic matter and modern examples  
398 have been found to contain DNA from various kinds of Bacteria and Archaea, many of which are  
399 involved in the N-cycle (Heim et al., 2017; Peng et al., in review). Phosphorous is a vital element  
400 for life and is found in high abundance in the Katanga malachite (Table 2), which is analogous to  
401 the presence of biological apatite that forms diagenetic rosettes with organic matter, carbonate,  
402 and quartz in Paleoproterozoic stromatolitic phosphorite (Papineau et al., 2016). Hence, high P in  
403 the Katanga malachite is further evidence for a biological origin of the organic matter that  
404 constitutes the arborescent structures. The new structures of organic matter that form arborescent  
405 morphologies in the geometric centers of Katanga malachite botryoids are therefore analogous to  
406 similar structures seen in deep-sea, deep crustal, and diagenetic settings. However, because  
407 malachite botryoids form in concretionary cavity structures from surface groundwater solutions  
408 in the absence of light, stromatolite morphologies in botryoidal malachite are unlikely to be  
409 evidence for phototrophy. Nevertheless, their occurrence in botryoidal crust is consistent with the  
410 non-biological decomposition and decarboxylation of biological organic matter and this  
411 occurrence in concretionary structures is another possible link with chemically-oscillating  
412 reactions.

413

414

**Implications**

415           The similarities between perfect patterns in chemically-oscillating reactions and those in  
416 botryoidal malachite are visually striking. Chemically-oscillating reactions produce self-similar  
417 patterns of circularly-concentric laminations spanning sizes between hundreds of microns to  
418 decimeter scales, identical to the shapes and size range of botryoidal malachite, which contains  
419 microscopic rosettes and macroscopic botryoids. Because these patterns are self-similar and span  
420 several orders of size dimensions, they can be referred to as fractal patterns. The geometric  
421 centers of malachite botryoids often contain dense arborescent or bulbous dendritic organic  
422 matter, which is implied as a major source of reactants, especially carboxyl, during the chemical  
423 oscillations. Depending on the availability of oxidants and halogens, chemically-oscillating  
424 reactions could occur spontaneously as a result of diagenetic biomass decomposition and its  
425 decarboxylation. Decarboxylation would occur during the putrefaction of biomass, which  
426 produces CO<sub>2</sub> and could have mixed with other sources of carbonate (such as seawater) to then  
427 precipitate as malachite. This could conceivably occur rapidly after a rise in alkalinity and freeze  
428 instantly after the passage of chemical waves. Chemically-oscillating reactions require organic  
429 acids of biological or non-biological origin, produce CO<sub>2</sub> bubbles and thus contribute to the  
430 carbon cycle. Therefore, botryoidal malachite and probably various other spheroidally-concentric  
431 sedimentological structures likely constitute signatures of decarboxylation reactions in aqueous  
432 environments. If sedimentological features do indeed arise from chemically-oscillating reactions,  
433 such signatures could be found to be ubiquitous during some periods of Earth history, for  
434 instance during the Paleoproterozoic, Neoproterozoic, and Late Paleozoic-Mesozoic, when  
435 environmental O<sub>2</sub> levels significantly increased, as well as on other ancient planetary surfaces as  
436 evidence of possible prebiotic chemical reactions.

437

438

### Acknowledgements

439 I acknowledge fruitful discussions on this topic with Z. She, K. Devine, J. Götze, G.  
440 Shields, N. Lane, E. Oelkers, R.M. Hazen, J. Cleaves, M. Chan, and T. Kee as well as continuing  
441 support from the LCN and UCL. Z. She and B. Shen are acknowledged for preparing solutions  
442 and providing preliminary trace element analyses. A.-L. Jourdan performed stable isotope  
443 analyses and G. Tarbuck conducted ICP-MS and ICP-OES analyses, both of whom are gratefully  
444 acknowledged. J.M. McArthur and two anonymous reviewers are kindly thanked for constructive  
445 comments that improved this manuscript.

446

447

448

### References

449

450 Agladze, K.I., Krinsky, V.I., and Pertsov, A.M. (1984) Chaos in the non-stirred Belousov-  
451 Zhabotinsky reaction is induced by interaction of waves and stationary dissipative  
452 structures. *Nature* 308, 834-835.

453 Akai, J., Akiyama, S., Tsuchiyama, A., and Akai, K. (2013) Ocean manganese nodules as  
454 stromatolite with a fractal like-signature. *Physics and Chemistry of the Earth* 58-60, 42-  
455 48.

456 Andrews, J.E., Kendall, A.C., and Hall, A. (2014) Microbial crusts with Frutexites(?) and iron  
457 staining in chalks: Albian-Cenomanian boundary, Hunstanton, UK. *Geological Magazine*  
458 152, 1-11. DOI: 10.1017/S0016756814000107

***Earth in five Reactions Special Collection***

Papineau

Revision 1

- 459 Belmonte, A. Ouyang, Q., and Flesselles, J.-M. (1997) Experimental survey of spiral dynamics  
460 in the Belousov-Zhabotinsky reaction. *Journal de Physique II*, EDP Sciences 7, 1425-  
461 1468.
- 462 Bernard, S., Benzerara, K., Beyssac, O., Menguy, N., Guyot, F., Brown, G.E. Jr., and Goffé, B.  
463 (2007) Exceptional preservation of fossil plant spores in high pressure metamorphic  
464 rocks. *Earth and Planetary Science Letters* 262, 257-272.
- 465 Brasier, M.D., Green, O.R., Lindsay, J.F., McLoughlin, N., Steele, A., and Stoakes, C. (2005)  
466 Critical testing of Earth's oldest putative fossil assemblage from the ~3.5 Apex chert,  
467 Chinaman Creek, Western Australia. *Precambrian Research* 140, 55-102.
- 468 Briggs, T.S. and Rauscher, W.C. (1973) An oscillating iodine clock. *Journal of Chemical*  
469 *Education* 50, 496.
- 470 Chou Chen, I., Kuksenok, O., Yashin, V.V., Moslin, R.M., Balazs, A.C., and Van Vliet, K.J  
471 (2011) Shape- and size-dependent patterns in self-oscillating polymer gels. *Soft Matter* 7,  
472 3141-3146.
- 473 Djokic, T., Van Kranendonk, M.J., Campbel, K.A., Walter, M.R., and Ward, C.R. (2017)  
474 Earliest signs of life on land preserved in ca. 3.5 Ga hot spring deposits. *Nature*  
475 *Communications*. DOI: 10:1038/ncomms15263.
- 476 Dodd, M.S., Papineau, D., She, Z., Manikyamba, C., Wan, Y., O'Neil, J., Karhu, J., Rizo, H.,  
477 Pirajno, F. (2019) Widespread occurrences of variably crystalline <sup>13</sup>C-depleted graphitic  
478 carbon in banded iron formations. *Earth and Planetary Science Letters* 512, 163-174.
- 479 Epstein, I.R., Kustin, K., De Kepper, P., and Orbán, M. (1983) Oscillating chemical reactions.  
480 *Scientific American*, 112-123.

***Earth in five Reactions Special Collection***

Papineau

Revision 1

- 481 Garcia-Ruiz, J.M., (1994) Inorganic self-organisation in Precambrian cherts. *Origins of Life and*  
482 *Evolution of the Biosphere* 24, 451-467.
- 483 Gaweda, A. and Rzymelka, J.A. (1992) Bituminous agates from rhyolites in the environs of  
484 Nowy Kosciol, Lower Silesia. *Mineralogia Polonica* 23, 73-84.
- 485 Götze, J. (2011) Agate – fascination between legend and science. In: Zenz, J. (ed.) *Agates III*.  
486 Bode-Verlag, 19-133.
- 487 Götze, J., Möckel, R., Vennemann, T., and Müller, A. (2015) Origin and geochemistry of agate  
488 in Permian volcanic rocks of the Sub-Erzgebirge basin, Saxony (Germany). *Chemical*  
489 *Geology* 428, 77-91.
- 490 Hartman, R.J., Kanning, E.W., and Klee, F.G. (1934) The Liesegang phenomenon applied to  
491 banded malachite. *Journal of Chemical Education* 11, 346-350.
- 492 Heim, C., Quéric, N.-V., Ionescu, D., Schafer, N., and Reitner, J. (2017) Frutexites-like  
493 structures formed by iron oxidizing biofilms in the continental subsurface (Äspö Hard  
494 Rock Laboratory, Sweden) *PLOS One*. DOI: 10.1371/journal.pone.0177542
- 495 Hemachandran, K. and Chetal, A.R. (1986) X-ray K-absorption study of copper in malachite  
496 mineral. *Physica Status Solidi* 136, 181-185.
- 497 Jakubowicz, M., Belka, Z., and Berkowski, B. (2014) Frutexites encrustations on rugose corals  
498 (Middle Devonian, southern Morocco): complex growth of microbial microstromatolites.  
499 *Facies* 60, 631-650.
- 500 Jamtveit, B. and Hammer, Ø (2012) Sculpting of rocks by reactive fluids. *Geochemical*  
501 *Perspectives* 1, 341-480

***Earth in five Reactions Special Collection***

Papineau

Revision 1

- 502 Jettestuen, E., Jamtveit, B., Podladchikov, Y.Y., deVilliers, S., Amundsen, H.E.F., and Meakin,  
503 P. (2006) Growth and characterization of complex mineral surfaces. *Earth and Planetary*  
504 *Science Letters* 249, 108-118.
- 505 Körös, E. and Orbán, M. (1978) Uncatalysed oscillatory chemical reactions. *Nature* 273, 371-  
506 372.
- 507 Lazar, I., Gradinaru, M., and Petrescu, L. (2013) Ferruginous microstromatolites related to  
508 Middle Jurassic condensed sequences and hardgrounds (Bucegi Mountains, Southern  
509 Carpathians, Romania). *Facies* 59, 359-390.
- 510 Liesegang, R.E. (1910) Die Entstehung der Achate. *Zentralblatt für Mineralogie* 11, 593-597.
- 511 Liesegang, R.E. (1915) Die Achate. Verlag von Theodor Steinkopff, Dresden und Leipzig, 122  
512 S.
- 513 Orbán, M., Kurin-Csörgei, K., Zhabotinsky, A.M., and Epstein, I.R. (2001) A new chemical  
514 system for studying pattern formation: Bromate-hypophosphite-acetone-dual catalyst.  
515 *Faraday Discussion* 120, 11-19.
- 516 Papineau, D., She, Z., and Dodd, M.S. (2017) Chemically-oscillating reactions during the  
517 diagenetic oxidation of organic matter and in the formation of granules in late  
518 Paleoproterozoic chert from Lake Superior, *Chemical Geology* 470, 33-54.
- 519 Papineau, D., De Gregorio, B.T., Fearn, S., Kilcoyne, D., Purohit, R., and Fogel, M.L. (2016)  
520 Nanoscale petrographic and geochemical insights on the origin of Paleoproterozoic  
521 stromatolitic phosphorites from Aravalli, India. *Geobiology* 14, DOI: 10.1111/gbi12164. 3-  
522 32.

***Earth in five Reactions Special Collection***

Papineau

Revision 1

- 523 Papineau, D., DeGregorio, B.T., Cody, G.D., O'Neil, J., Steele, A., Stroud, R.M., and Fogel,  
524 M.L. (2011) Young poorly crystalline graphite in the >3.8 Gyr old Nuvvuagittuq banded  
525 iron formation, *Nature Geoscience* 4, 376-379.
- 526 Peng, X. Guo, X., Czaja, A., and Papineau, D. (in review in *Science Advances*) Endolithic life in  
527 metamorphic ocean crust. 24 pp.
- 528 Plet, C., Grice, K., Pages, A., Ruebsam, W., Coolen, M.J.L., and Schwark, L. (2016)  
529 Microbially-mediated fossil-bearing carbonate concretions and their significance for  
530 paleoenvironmental reconstructions: A multi-proxy organic and inorganic geochemical  
531 appraisal. *Chemical Geology* 426, 95-108.
- 532 Richter-Feig, J., Möckel, R., Götze, J., Heide, G. (2018) Investigation of fluids in  
533 microcrystalline and microcrystalline quartz in agate using thermogravimetry-mass-  
534 spectrometry. *Minerals* 8, 72. DOI: 10.3390/min8020072.
- 535 Schopf, J.W. and Kudryavtsev, A.B. (2009) Confocal laser scanning microscopy and Raman  
536 imagery of ancient microscopic fossils. *Precambrian Research* 173, 39-49.
- 537 Seilacher, A. (2001) Concretion morphologies reflecting diagenetic and epigenetic pathways.  
538 *Sedimentary Geology* 143, 41-57.
- 539 Turing, A.M. (1952) The chemical basis of morphogenesis. *Phil. Trans. Royal. Soc. London* 237,  
540 37-72.
- 541 Walter, M.R. and Awramik, S.M. (1979) Frutexites from stromatolites of the Gunflint iron  
542 formation of Canada, and its biological affinities. *Precambrian Research* 9, 23-33.
- 543 Zhabotinsky, A.M. (1991) A history of chemical oscillations and waves. *Chaos* 1, 379-386.
- 544 Zaikin, A.N. and Zhabotinsky, A.M. (1970) Concentration wave propagation in two-dimensional  
545 liquid-phase self-oscillating system. *Nature* 225, 535.



546

547

548

549

550

551

552

553

554

555

556

557 **Figure 1: Morphological comparison of sub-millimetric to decimetric self-similar patterns**  
558 **in chemically-oscillating experiments (left, orange-blue coloured liquid in one-decimetre**  
559 **diameter Petri dishes) and in botryoidal malachite (right, various specimens from private**  
560 **collections). In B-Z experiments, none of the patterns were induced, e.g. with a tool. a-b)**  
561 **cavity shapes with imperfect to perfect concentric equidistant laminations associated with**  
562 **spheroidal to ellipsoidal concentric spots, c-d) globular growth patterns without or with**  
563 **few concentric laminations and sometimes with zebra-like bands (white arrows), e-f) spots**  
564 **with perfect to slightly imperfect equidistant laminations (yellow arrows show CO<sub>2</sub>**  
565 **bubbles), g-h) linear to wavy and columnar turbinate (stromatolite-like) equidistant**  
566 **laminations showing colour gradients along chemical waves and laminations as well as**  
567 **spotted patterns (white arrows), i-j) spotted pattern (white arrow) in background (with a**

***Earth in five Reactions Special Collection***

Papineau

Revision 1

568 **second-order oscillation and inverted textures in the B-Z reaction) and with perfect to**  
569 **imperfect concentric laminations from the micrometre to centimetre scales.**

570

571 **Figure 2: Petrographic context of organic matter with bulbous dendritic morphology**  
572 **located in the geometric centre of self-similar malachite botryoids. a-c) Transmitted light**  
573 **images through thin sections showing the location of *Frutexites* (black organic matter in**  
574 **red boxes) and the turbinate-like stromatolite textures of green to black malachite from**  
575 **Katanga. d) opaque organic matter in the centre of radiating acicular malachite, e)**  
576 **transmitted and reflected light image of dendritic organic matter with cavities located in**  
577 **the geometric centre of concentric malachite laminations, f) dendritic and layered organic**  
578 **matter located in the geometric centres of several concentrically-laminated spots of**  
579 **malachite (white arrows), g) micro-Raman image of the organic matter in (f) associated**  
580 **with quartz and anatase, h) Raman spectra of the minerals shown in (g) showing two types**  
581 **of organic matter.**

582

**Table 1:** comparison of morphological traits between the self-similar patterns in malachite and in chemically-oscillating reactions.

<b>Morphological trait</b>	<b>Chemically-oscillating reaction</b>	<b>Malachite</b>
Circularly concentric and equidistant laminations	Fig. 1a (pl. 2, 3,) and Fig. 1e (pl. 1, 2)	Fig. 1b (pl. 1-3) and Fig. 1f (pl. 1-3)
Spots with concentric equidistant laminations spanning sizes from sub-millimeter to decimeter	Fig. 1a (pl. 2) and Fig. 1i (pl. 3)	Fig. 1b (pl. 2) and Fig. 1j (pl. 3)
Cavity-shaped structures formed from the destructive interference of chemical waves	Fig. 1a (pl. 1, 3)	Fig. 1b (pl. 2)
Asymmetric (sub-ellipsoidal) concentric laminations	Fig. 1a (pl. 1, 4), Fig. 1e (pl. 3), and Fig. 1i (pl. 4)	Fig. 1b (pl. 1, 3) and Fig. 1h (pl. 3)
Parallel-layered to wavy patterns with intersecting oxidation spots	Fig. 1g (pl. 1, 2)	Fig. 1f (pl. 1) and Fig. 1j (pl. 1-3)
Columnar-turbinate laminated pattern (stromatolite-like)	Fig. 1g (pl. 4.)	Fig. 1h (pl. 1-3)
Colour gradients in laminations	Fig. 1c (pl. 3, 4) and Fig. 1g (pl. 3)	Fig. 1b (pl. 1-3) and Fig. 1j (pl. 1)
Diffused spotted texture with a distinct periodicity than laminations	Fig. 1i (pl. 1, 2)	Fig. 1h (pl. 3) and Fig. 1j (pl.1-3)
Globular texture with three-dimensional grape-like morphology	Fig. 1c (pl. 1-4)	Fig. 1d (pl. 1-3)

**Table 2: Bulk geochemical composition of Katanga malachite\***

	ppb	ppm	%
Al		401.50	
As		33.28	
Ba		39.81	
Be	11274.0		
Bi	4.8		
Ca		38.88	
Cd	1.0		
Co	199466.9		
Cr	561.7		
Cu			55.27
Fe		85.05	
K		75.23	
Mg		163.28	
Mn		585.36	
Na		24.07	
Ni		17.97	
P			4.28
Pb		3.44	
Ti		6.91	
V		171.55	
Zn		890.94	
Sc	1907.9		
Y	6657.0		
La	369.7		
Ce	343.5		
Pr	136.2		
Nd	761.6		
Sm	363.2		
Eu	122.1		
Gd	732.9		
Tb	137.5		
Dy	889.3		
Ho	197.0		
Er	544.2		
Tm	71.5		
Yb	455.9		
Lu	73.1		
Th	313.7		
Br	10864.8		
I	1102.7		
$\delta^{13}\text{C}_{\text{carb}}$	-10.6‰		
$\delta^{18}\text{O}_{\text{carb-PDB}}$	-5.1‰		
$\delta^{13}\text{C}_{\text{org}}$	-28.6‰		

\* Concentrations in ppb are from the ICP-MS while those in ppm and % are from the ICP-OES.



